Particle transport via gas puff modulation experiments in JET

A. Salmi[1], T. Tala[1], C. Bourdelle[2], P. Mantica[3], L. Meneses[4], S. Mordjick[5], H. Bufferand[2], M. Clever[6], J. Svensson[7], P. Tamain[2], M. Groth[8], J. Hillesheim[9], C. Maggi[10], M. Maslov[9], V. Naulin[11], J. Juul Rasmussen[11], G. Sips[12], A. Sirinelli[13], M. Tsalas[14], H. Weisen[15], M. Wischmeier[10] and JET-EFDA contributors*

JET-EFDA, Culham Science Centre, Abingdon, OX14 3DB, UK

[1]VTT, Espoo, Finland; [2]IRFM-CEA, Saint Paul lez Durance, France; [3]IFP, CNR-ENEA, Milan, Italy; [4]IST, Lisbon, Portugal; [5]College of William & Mary, Virginia, USA; [6]FZJ, Jülich, Germany, [7]IPP, Greifswald, Germany, [8]Aalto University, Helsinki, Finland; [9]CCFE, Abingdon, UK; [10]IPP, Garching, Germany; [11]DTU Physics, Lyngby, Denmark; [12]EFDA CSU, Culham, [13]ITER, France, [14]DIFFER, Nieuwegein, Netherlands; [15]CRPP, Lausanne, Switzerland.

** See the Appendix of F. Romanelli et al., Proc. 24th IAEA FEC, San. Diego 2012*

ABSTRACT

Plasma fuelling is mandatory for maintaining fusion reactions in fusion power plants. The high temperature and high density SOL of burning plasmas are expected to significantly reduce the efficiency of gas puff fuelling. It is important to investigate how todays high performance H-mode plasmas are fuelled through the pedestal to understand whether ITER and DEMO can rely on gas injection as the main fuelling scheme.

The recently upgraded reflectometer diagnostics in JET together with modulated gas puff injection technique are utilised to extract the D and V profiles from a 3-point collisionality scan in L-mode. Furthermore, proof-of-principle tests in H-mode are made with several gas injection locations and frequencies to identify whether modulated density signals are detected and which settings are optimal to use in future parameter scans.

GAS MODULATION LOCATIONS AND THE MEASURED DENSITY MODULATION IN A JET H-MODE PLASMA

The H-mode discharges in this proof-of-principle experiment are run in the corner configuration with low triangularity, Bt=2.7T, Ip=2.0MA, ne0=6x1019m-3, Te0=3.5keV. Figure 2 illustrates the various gas injection locations used in these discharges on poloidal plane. The top and midplane GIMs can be considered as point sources while the ones at the divertor are nearly axisymmetric. GIM 12 was on in all discharges with constant gas rate of ~1.5e22 1/s while the others were modulated (one at a time) using 2-4 Hz rectangular waveform with 50% duty cycle going from 0 to ~1.5e22 1/s. Note that due to the gas modulation the plasma boundary position given by the fast, magnetics only, EFIT was found to oscillate with an amplitude of ~1mm.

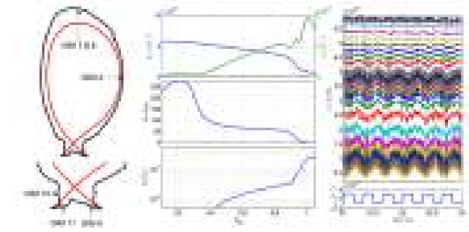

Figure: (left)gas injection locations on poloidal plane (middle) electron density profile and the modulation amplitude and phase profiles at 3 Hz for #85231 (right) gas modulation waveform and the temporal density traces from reflectometer.

REFLECTOMETER AGREES V THOMSON

The principal quantity of interest, electron density, is measured with a multi-band reflectometer capable of good spatial and temporal resolution. As shown in the comparison the High Resolution Thomson Scattering (HRTS) data agrees nicely with the reflectometer measurements. The rather flat core density present in these discharges is problematic for the reflectometer and inside R~3.3 m the data becomes unreliable. On the other hand, the steep gradient region and the SOL density down to about 2e17 m-3 are well covered by the reflectometer. Interestingly, HRTS data indicates increasing amplitude in the core.

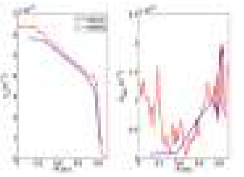

D and v deduced from electron density evolution

In interpreting the measurements we assume that the electron density evolution follows the usual 1.5D equation for non-cylindrical and axisymmetric plasmas:

$$\frac{\partial}{\partial t}(V' n_e) = \frac{\partial}{\partial \rho}\left[V' \langle(\nabla\rho)^2\rangle \left(D\frac{\partial n_e}{\partial \rho} - v n_e\right)\right] + V' S$$

We utilise this equation in two ways to deduce the underlying transport.

1. We solve it inside a loop with nonlinear optimisation algorithm adjusting the transport coefficients D and v until best fit against measurements in χ^2 sense is found simultaneously for the modulated amplitude, phase and the steady state profiles. Flux boundary condition is used at the outer boundary. The source profiles are given by PENCIL and FRANTIC codes.
2. For any periodic perturbation with time independent transport one can use the measured amplitude and phase profiles of the perturbation to calculate the transport coefficients D and v [7]. In Ref. [7] these formulas were derived in a cylindrical plasma approximation. Here, we write D and v starting from the more general geometry included in the above equation while also retaining the source term. Using the ansatz $n_e(\rho,t) = n_0(\rho) + A(\rho)\sin(\omega t - \varphi(\rho))$ together with $S(\rho,t) = S_0(\rho) + A_s(\rho)\sin(\omega t - \varphi_s)$ and a little algebra we arrive at:

$$D = -\omega\frac{Y\sin\varphi + X\cos\varphi}{A\varphi' V' \langle(\nabla\rho)^2\rangle}, \quad v = -\omega\frac{(A'Y - \varphi' A X)\sin\varphi + (\varphi' A Y + A' X)\cos\varphi}{A^2\varphi' V' \langle(\nabla\rho)^2\rangle}$$

$$X = \int V'\left(A\cos\varphi + \frac{A_s}{\omega}\sin\varphi_s\right)d\rho, \quad Y = \int V'\left(A\sin\varphi - \frac{A_s}{\omega}\cos\varphi_s\right)d\rho$$

PERTURBATIVE D & V IN H-MODE

The adjacent figure summarises the D and v profiles for the full H-mode data set (#85228 - #85232) using analytic equations while neglecting any modulated source terms (valid inside 0.8). One can observe in the top left and top right frames that in cases where the same modulation frequency was used the same amplitude profile is obtained with good accuracy. Especially the top right frame is of interest as the green lines represent different top GIMs. One can thus conclude that no non-axisymmetric effects are observed in the density data and that the data is well reproducible. Another clear observation is that the measured amplitude increases with decreasing frequency (as expected) while somewhat puzzling finding is that the decay length of the amplitude does not appear to decrease with increasing frequency. Furthermore, counter to expectations, the derived convective velocity is outwards. This is not compatible with the peaked steady state profile that in fact requires inward convection given the relatively small central fuelling from NBI.

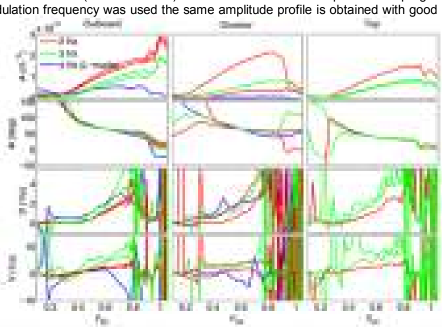

D & V FROM ITERATIVE TRANSPORT OPTIMISATION

- Source profile shapes are obtained from PENCIL [12] and FRANCTIC in steady state conditions
- The rapidly decaying amplitude and the flat phase are not matched exactly without outward convection.
- Same conclusion was obtained also in ASTRA transport code simulations.

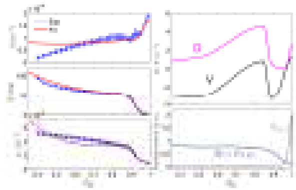

Figure: Optimal fit that simultaneously matches amplitude, phase and steady state profiles using iterative approach for solving D and v profiles.

ELMs AND SAWTEETH

- Both sawteeth and ELMs are clearly visible on top of the gas modulation
- The sawtooth frequency is roughly ~4 Hz irrespective of the modulated GIM or the modulation frequency
  - Gas puff modulation near 4 Hz can not be used due to strong interference
- ELMs occur at ~50 Hz and consequently appear several times within each modulation cycle
  - D&V are thus ELM-averaged quantities
  - ELM frequency is modulated by about ~10% due to the gas modulation

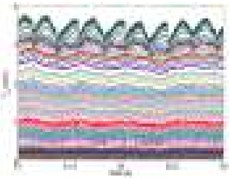

Figure: (left) Electron temperature illustrating various frequencies present in the in the data (right) conditionally averaged electron density for #85232 over 8s time window

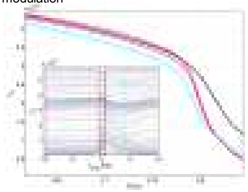

COMPLEX PARTICLE SOURCE

- Incompatibility between perturbative and particle balance D and V could also be due to too simple 1D sources used
- Tomographic inversion [8] of KL11 [9] data (Dα video, see figure) in the Minerva framework [10] hints of more complex 2D source (see figure)

Some observations

- *frame b:* modulated emission occurs in three distinct regions
  1) direct source aligned with LFS separatrix
  2) recycling source on the inner divertor apron
  3) volume source just left of the X-point
- HFS emission comes ~40 ms after the LFS emission
- Volume emission is in anti-phase with the LFS emission
- Both steady state and modulated emission from GIM 4 is stronger on the LFS
- Detailed future SOL modelling together with this data is hoped to provide valuable information about particle sources

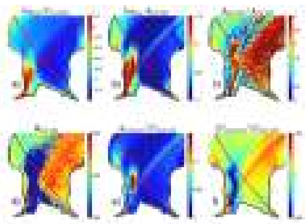

Figure: Modulated and steady state intensity profiles of Dα light from GIM4 and GIM8 modulation phases. Note that GIM 12 was constantly on in both cases.

L-MODE COLLISIONALITY SCAN

- Discharges #79811, #79814, #79815 in JET L-mode form a dimensionless 3-point collisionality scan which was achieved by changing temperature with NBI while keeping the density constant
- Calculated D&V profiles are roughly the same inside 0.6 where the modulated particle source is expected to be very small. Even outside there is no trend.
- This finding is consistent with the earlier experimental database study on JET [6] where in L-mode no
- The result was also confirmed by a gyrokinetic quasi-linear analysis using QuaLiKiz [12] that found no trends within the scan.
  - However, it is noted that weak collisionality dependence in the relevant L-mode parameter range was found with QuaLiKiz when using artificial parameters nulling the small but unavoidable Te/Ti changes in the experimental scan.

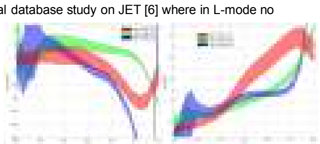

CONCLUSIONS AND FUTURE WORK

- Particle transport in L-mode does not show strong correlation with collisionality
- Proof-of-principle H-mode experiment successfully produced clear and repeatable density perturbations using the KG10 reflectometer
- GIM 4 provides the largest density modulation for a given gas rate (3D effect?)
- Simple transport models do not fully explain the measured density behaviour (perturbative D and V are different from particle balance D and V)
- Analysis of new JET experiments from last week

ACKNOWLEDGEMENTS

This work was supported by EURATOM and carried out within the framework of the European Fusion Development Agreement. The views and opinions expressed herein do not necessarily reflect those of the European Commission.

REFERENCES

[1] K.W. Gentle et al 1992 NF 32 217
[2] J O'Rourke et al 1993 PPCF 35 585
[3] K. Nagashima et al 1993 NF 33 1677
[4] D.R. Baker et al 1998 NF 38 485
[5] A. Sirinelli et al 2010 RSI 81 10D939
[6] H. Weisen et al 2005 NF 45
[7] H Takenaga et al 1998 PPCF 40 183
[8] J. Svensson 2011 EFDA–JET–PR(11)24
[9] A. Huber et al 2012 RSI 83
[10] J. Svensson et al 2007 Proc. IEEE WISP
[11] R. Pasqualotto et al 2004 RSI 75
[12] C.D. Challis et al 1989 Nucl. Fusion 29 563
[13] C. Bourdelle et al 2007 PoP 14, 112501